J Inno Sci Eng, 2020, 4(2): 84-95
https://doi.org/10.38088/jise.731126

Research Article

TiB_2 Thin-Film Coated Glass and High-Speed Steel (HSS) in Applications of Radiation Shielding Technology

Mehmet Büyükyıldız [1*], Ahmet Turan [2], Tolga Tavşanoğlu [3], Erdem Şakar [4], Onuralp Yücel [5], Murat Kurudirek [4]

[1] *Faculty of Engineering and Natural Sciences, Department of Physics, Bursa Technical University, 16310 Bursa, Turkey,*

[2] *Faculty of Engineering, Chemical and Process Engineering Department, Yalova University, 77200 Yalova, Turkey*

[3] *Department of Metallurgical and Materials Engineering, Mugla Sitki Kocman University, 48000 Kotekli, Mugla, Turkey*

[4] *Faculty of Science, Department of Physics, Atatürk University, 25240 Erzurum, Turkey*

[5] *Department Faculty of Chemical and Metallurgical Engineering, Metallurgical and Materials Engineering Department, Istanbul Technical University, 34469, Maslak, Istanbul, Turkey*

Cite this paper as:
Buyukyildiz, M., Turan, A., Tavsanoglu, T., Sakar, E., Yucel, O., Kurudirek, M.(2020). TiB_2 Thin-Film Coated Glass and High-Speed Steel (HSS) in Applications of Radiation Shielding Technology. Journal of Innovative Science and Engineering. 4(2): 84-95

*Corresponding author: Mehmet BUYUKYİLDİZ,
E-mail: mehmet.buyukyildiz@btu.edu.tr
Tel: +90 (224) 3003348

Received Date: 02/05/2020
Accepted Date: 13/07/2020

Abstract

TiB_2 (titanium diboride) is a transition metal boride with remarkable properties and, its thin-film coatings can be deposited on various substrates to develop the wear resistance properties of substrates. Radiation interaction properties of TiB_2 coated glass and HSS are very significant as well for shielding applications and it has not been investigated so far. In this work, linear attenuation coefficient (μ), half-value layer (HVL), tenth-value layer (TVL) and mean free path (MFP) of TiB_2 coated glass and HSS (AISI-M2) were measured using a ^{133}Ba radioactive point source at energies 80.8, 276.4, 302.8, 356 and 383.8 keV. A comparison has been made with some radiation shielding concretes with respect to MFP. Energy absorption and exposure buildup factors (EABF and EBF) of composites were also calculated in the experimental energy region 50 – 500 keV. TiB_2 coated glass and HSS were found to be better radiation shielding materials than the standard shielding concretes concluding that they can be further developed for radiation shielding applications.

Keywords: Radiation shielding, Thin film coating, TiB_2.

1. Introduction

TiB_2 is a transition metal boride and has significant properties such as physical, mechanical, and chemical. It has high hardness, strength, melting point (about 3225 °C), and wears resistance. In addition, it has high thermal and electrical conductivity with high durability for chemical materials and molten metals. Its crystal structure is hexagonal and it has a covalent bond type (space group of P6/mmm). The main application areas of TiB_2 are armors for impact, cutting tools, some evaporation crucibles, coatings for wear and electrolysis cathodes based on aluminum [1, 5].

Some studies about TiB_2 thin films have been reported mainly on the mechanical and tribological characteristics in the literature. Huang et al. studied on the production of ultrathin TiB_2 films (5 nm) on the magnetic layers as a protective overcoat and, they found that this these ultrathin TiB_2 films protect underlying magnetic layers up to 400 °C from oxidation [6]. Mishra et al. disputed the results of a magnetron sputtering deposition study on nanocrystalline TiB_2 thin films [7]. They obtained a maximum hardness value of 36 GPa on thin films. TiB_2 thin films, which are coated by dc-magnetron sputtering, were studied by Sanchez et al. on behalf of structural and mechanical features [8]. They found that increasing film density increased the mechanical properties of coated thin films. 23±3 GPa hardness and 200±20 GPa elastic modulus values were determined for TiB_2 thin film which has a density of 4.9 g/cm^3. Xia et al. worked on the adhesion properties of TiB_2 thin films by Ti interlayer films on 316L stainless steel substrates. Ti/TiB_2 multilayered films showed better adhesion properties (maximum 24 N) than monolayer TiB_2 thin films [9]. Zhang et al. investigated the influences of negative bias potential and deposition temperature on the high power impulse magnetron sputtering of TiB_2 thin films [10]. They found that hardness and elastic modulus firstly increased up to -100 V for hardness (52.7 GPa) and up to -150 V for elastic modulus (306.4 GPa) bias voltage values. And it began to decrease after those voltage values at 200 °C. However, those mechanical properties showed a continuous increase with decreasing voltage value at 300 °C.

Radiation shielding has been the subject of research in various materials such as concretes [11-13], glass systems [14-17], steel [18-22], cement mixture [23] and basalt rock samples [24]. However, to the best of our knowledge radiation shielding properties of TiB_2 coated glass and HSS have not been investigated yet. Thus, we have embarked on investigating TiB_2 coated glass and HSS with respect to their radiation shielding properties for energetic gamma rays. In this respect, linear attenuation coefficient (LAC, μ), mean free path (MFP), half-value layer (HVL), and tenth-value layer (TVL), and buildup factors, which are relevant parameters in radiation shielding, were calculated in the present work. Results of this work were also compared with important standard shielding concretes in terms of radiation shielding.

2. Material and Methods

The Beer–Lambert law was used to determine the lineer and mass attenuation coefficient of the studied materials at any photon energy as:

$$I = I_0 e^{-\mu x} = I_0 e^{-\mu_m t} \quad (1)$$

$$\mu_m = (\frac{\mu}{\rho}) = \frac{\ln(I_0/I)}{\rho t} \tag{2}$$

I_O and I are defines as unattenuated and attenuated (for any measurement) photon intensities. μ (cm^{-1}) and μ_m ($cm^2.g^{-1}$) are known as linear and mass attenuation coefficients. x (cm) and t ($g.cm^{-2}$) are described as the thickness and sample mass thickness (the mass per unit area), and ρ ($g.cm^{-3}$) is the density of material. Also, the total mass attenuation coefficient μ_m can be calculated for any composite via mixture rule:

$$\mu_t = \left(\frac{\mu}{\rho}\right) = \sum_i w_i (\mu/\rho)_i \tag{3}$$

where w_i is the weight fraction of the ith constituent element , $w_i = \frac{n_i A_i}{\sum_i n_i A_i}$ A_i is the atomic weight of the ith element, and n_i is the number of atoms of ith constituent element in the composite [25]. After the linear attenuation coefficient is determined, HVL (cm) and TVL (cm) can be calculated by using the equation:

$$HVL = \frac{\ln(2)}{\mu} = \frac{0.693}{\mu} \quad \text{and} \quad TVL = \frac{\ln(10)}{\mu} = \frac{2.302}{\mu} \tag{4}$$

$$MFP = \frac{1}{\mu} \tag{5}$$

The buildup factors are the correction factors for Lambert-Beer Law, they characterize the distribution of photon flux in the interacting material. And they are significant parameters in dosimetry, therapy and, shielding applications. The buildup factors for any composite material can be calculated by the well-known G–P fitting method, and this procedure was referred to previously in the literature [24, 26-28]. In this point, Z_{eq} was firstly computed via the following equation:

$$Z_{eq} = \frac{Z_1(\log R_2 - \log R) + Z_2(\log R - \log R_1)}{\log R_2 - \log R_1} \tag{6}$$

Z_1 and Z_2 represent the atomic numbers of the elements corresponding to the ratios R_1 and R_2, respectively, and R is the ratio for the chosen building materials at a specific energy: $R = (\mu/\rho)_{Compton} / (\mu/\rho)_{Total}$ by using WinXCom program [29]. Then G–P fitting parameters were computed using a similar interpolation procedure and ANSI/ANS-6.4.3 standard reference database was used to obtain values of elements. Finally, these G–P fitting parameters were used to calculate the EBFs and EABFs of the materials by using the G-P fitting formula [30]:

$$\mathrm{B(E,X)} = 1 + \frac{b-1}{K-1}(K^x - 1)\ for\ K \neq 1 \quad (7)$$

$$\mathrm{B(E,X)} = 1 + (\mathrm{b} - 1)\mathrm{x}\ for\ K = 1 \quad (8)$$

where,

$$\mathrm{K(E,x)} = cx^a + d\frac{\tanh\left(x/X_k - 2\right) - \tanh(-2)}{1 - \tanh(-2)} \quad for\ x \leq 40\ mfp \quad (9)$$

E is the energy of incident photon, X is the penetration depth in mfp (cm). The symbols of a, b, c, d and X_k are the G-P fitting parameters and b is the buildup factor at 1 mean free path (mfp). And the K gives the photon dose multiplication and the change in the shape of the spectrum.

TiB_2 thin-film coatings were performed on AISI-M2 grade high-speed steel and glass substrates by using the DC magnetron sputtering system (HEF TSD-350 PECVD) (Figure 1) [31]. TiB_2 sputtering target was produced "in-house". It was designed and manufactured at Istanbul Technical University, Metallurgical and Materials Engineering Department, Macro to Nano Research Group Laboratories by SPS Syntex (SPS-7.40MK-VII) brand spark plasma sintering apparatus by using H. C. Starck-Grade D TiB_2 powders. The target was produced by the joining of sintered TiB_2 parts (theoretical density of 73%) on an electrolytic quality copper plate. It was round-shaped and having a diameter of 150 mm as well as a thickness of 7 mm (5 mm TiB_2 +2 mm copper plate). Materials thicknesses were changed as 0.10-0.19 cm. The detailed information about the manufacturing of target material can be found elsewhere [32]. An ultrasonic bath was done for the pre-cleaning of substrates in ethanol media before introducing into the deposition chamber of the sputtering apparatus. Experimental parameters of thin-film coating experiments can be seen in Table 1.

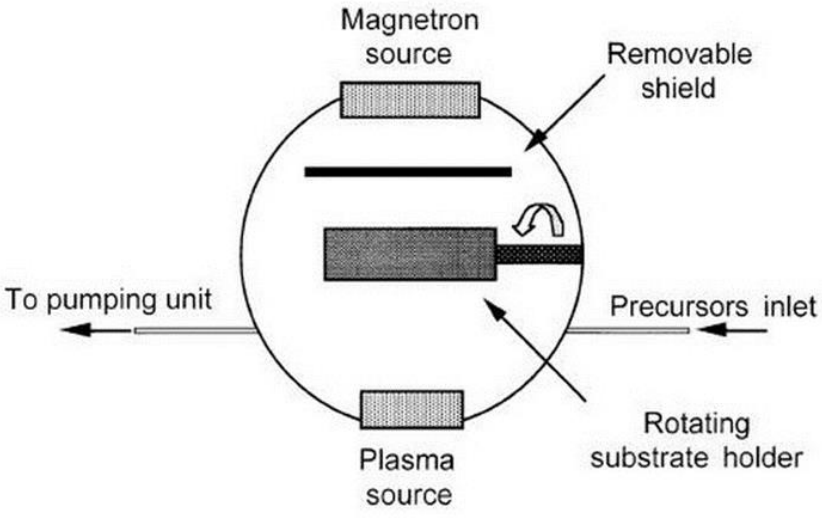

Figure 1. Schematic figure of the deposition reactor [32]

Table 1. Sputtering conditions for the deposition of TiB_2 films

Initial Pressure	Working Pressure	Ar Gas Flow	Deposition Temperature	Sputtering Power	Deposition Time
1 x 10^{-5} Pa	0.2 Pa	40 cm^3/min	250 °C	200 W	20, 30 min

TiB_2 thin-film coatings were deposited on the mirror-polished HSS and glass substrates. Deposition on HSS substrate was performed for 20 minutes whilst deposition durations were applied for 20 and 30 minutes on glass substrates. Micrographs of deposited thin films were taken by using JEOL JSM 7000F scanning electron microscope (SEM). It was used for the semi-quantitative energy-dispersive X-ray spectroscopy (EDS) analysis of the coatings as well.

To determine radiation interaction parameters, measurements were made at gamma energies of 80.8, 276.4, 302.8, 356 and 383.8 keV using a 10mCi ^{133}Ba radioactive point source. In order to detect gammas, an HPGe detector was used. For detector, the active area is 200 mm^2, it has Be window with a thickness of 0.127 mm, the radius is 13.97 mm, dead layer thickness is 500 Å, Ge crystal with a thickness of 7 mm, a radius of 7.981 mm, the detector bias voltage is 1500 V, and resolution is almost ~182 eV at 5.9 keV. Measurements were taken three times to obtain the average values and standard deviation (average±std deviation). A typical spectrum of gamma rays with and without attenuation is shown in Figure 2.

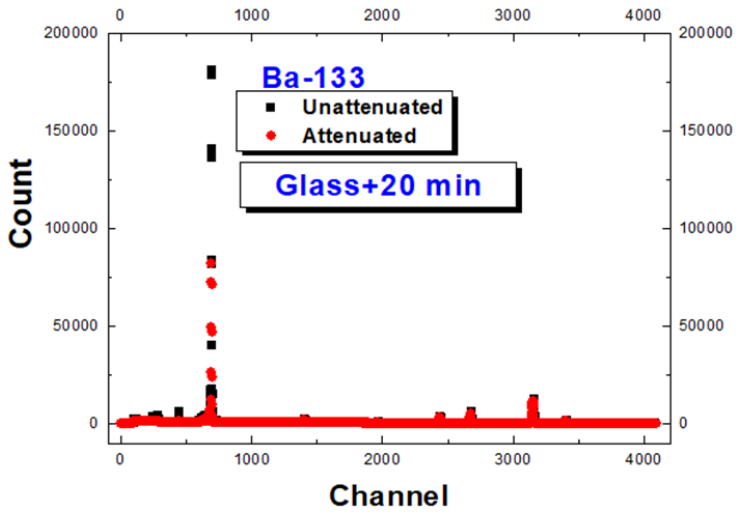

Figure 2. A typical spectrum of gamma rays with and without attenuation.

3. Results and Discussion

TiB_2 thin films were successfully deposited on HSS and glass substrates. TiB_2 thin-film coating on the HSS substrate (Figure 3) was applied for 20 minutes and, it had an average thickness of 135.5 nm. Fig. 4 shows TiB_2 thin-film coatings on glass substrates for a duration of 20 minutes and 30 minutes deposition. The Semi-quantitative composition of TiB_2 thin-film coatings is given in Table 2.

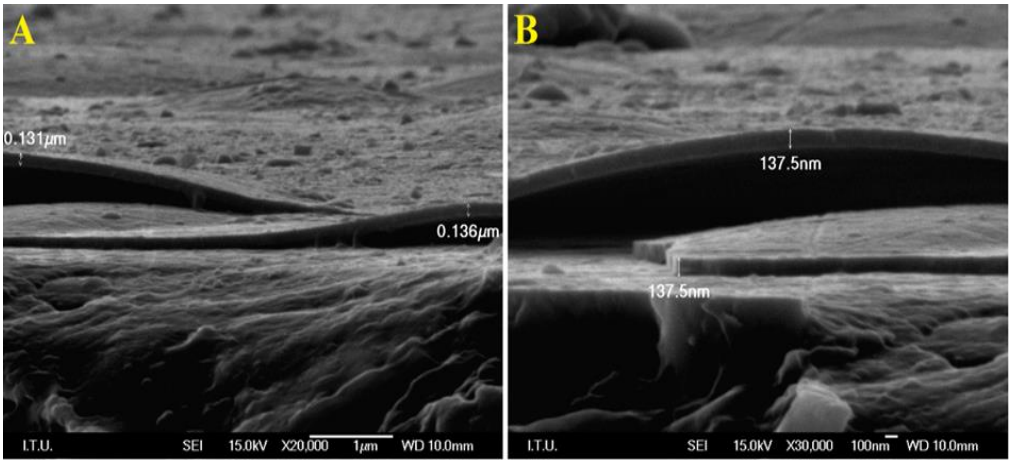

Figure 3. TiB_2 thin-film coating on HSS substrate for 20 minutes deposition duration; (A) at 20,000X and (B) at 30,000X magnification.

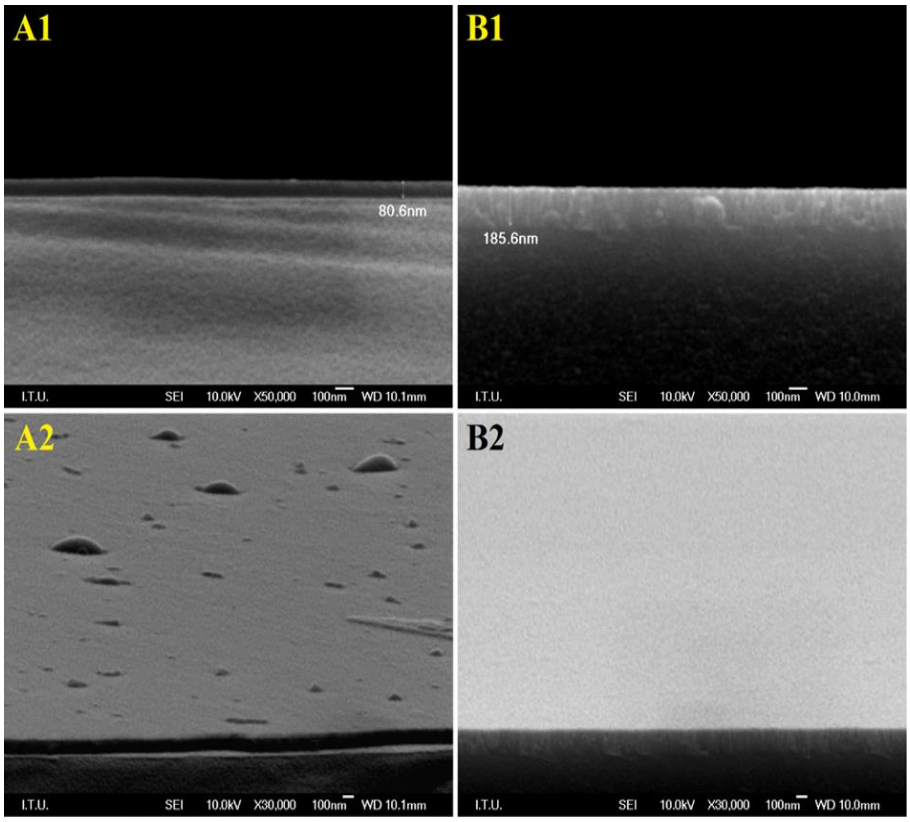

Figure 4. TiB_2 thin-film coatings on glass substrates; (A1) for 20 minutes and (B1) for 30 minutes deposition durations. (A2) and (B2) are the angular micrographs of corresponding coatings.

Table 2. Chemical compositions (EDS) of the substrates and TiB_2 thin-film coated substrates with increasing coating duration.

Material	**B**	**C**	**O**	**Ca**	**Ti**	**V**	**Cr**	**Fe**	**Pt**
HSS	-	6.43	-	-	-	1.73	15.37	73.46	3.00
HSS + 20 min Coating	24.35	11.50	19.88	0.50	6.26	-	2.87	30.92	3.71
	B	**C**	**O**	**Na**	**Mg**	**Si**	**Ca**	**Ti**	**Pt**
Glass	-	-	48.73	10.02	2.51	32.61	4.42	-	1.73
Glass + 20 min Coating	25.96	22.16	35.39	2.48	0.54	6.97	1.02	3.62	1.83
Glass + 30 min Coating	17.66	-	35.60	2.46	-	6.85	-	24.63	12.81

Average thickness values were found to be 80.6 nm and 185.6 nm for the TiB_2 deposition on glass substrate for 20 minutes and 30 minutes, respectively. It was clearly seen that increasing deposition duration increased the thickness of TiB_2 thin-films on the glass substrate. The thickness difference of TiB_2 thin-films on HSS and glass substrates deposited both for 20 minutes with the same conditions is believed to occur because of the mismatch in the mechanical properties. TiB_2 adhered more easily to HSS which has high hardness and elastic modulus whereas the adhesion was more difficult in glass which is a relatively softer material compared to HSS and has lower elasticmodulus.

The obtained values of the linear attenuation coefficient, half-value layer, and tenth value layer are listed in Table 3. Results are given as average values along with standard deviation. It has been observed that the linear attenuation coefficients decreased and the HVL (cm) and TVL (cm) increased as the gamma energy increases due to the higher penetration of high energy gamma rays (Table 3). HSS was found to have the highest values of linear attenuation coefficients among the investigated materials at all energies considered. In general, it has been noted that TiB_2 coating on HSS slightly decreased the radiation attenuation and TiB_2 coating on glass increased the radiation attenuation. HSS, glass and TiB_2 coated materials were compared to the concretes in terms of the mean free path (cm), which is representing the average distance between two successive interactions of gamma rays (Table 4). It is seen from the Table 4 that HSS and HSS+20 min TiB_2 have shown better radiation shielding than all concretes while glasses with TiB_2 have shown better radiation shielding than ordinary and hematite-serpentine concretes. The mass attenuation coefficient takes into account phase difference, so it is more useful than linear attenuation coefficient in terms of shielding. Figure 5 shows the mass attenuation coefficients (μ/ρ) of HSS, glass (with and without TiB_2), ordinary and hematite-serpentine concretes in the continuous energy region 10^{-2}-10^{3} MeV. Results revealed that HSS has the highest radiation attenuation in the whole energy region because of its high heavy metal contents such as iron and chromium in general. Also, it has been seen that except for glass with TiB_2 (20 min) all materials have better shielding than the ordinary concrete in the continuous energy range due to lower values of mean free paths.

Table 3. μ, HVL (cm) and TVL (cm) of the materials.

	Linear attenuation coefficient (μ)				
Energy (keV)	HSS	HSS + 20min	Glass	Glass + 20 min	Glass + 30 min
80.8	4.598±0.034	4.612±0.002	0.505±0.067	0.475±0.013	0.462±0.017
276.4	0.939±0.043	0.877±0.013	0.379±0.010	0.390±0.112	0.398±0.07
302.8	0.807±0.021	0.806±0.035	0.331±0.026	0.332±0.011	0.321±0.03
356	0.750±0.030	0.746±0.007	0.201±0.033	0.278±0.012	0.284±0.019
383.8	0.726±0.047	0.692±0.003	0.174±0.128	0.242±0.037	0.233±0.020
	Half value layer (HVL)				
Energy (keV)	HSS	HSS + 20min	Glass	Glass + 20 min	Glass + 30 min
80.8	0.151±0.001	0.150±0.0001	1.384±0.184	1.460±0.041	1.502±0.054
276.4	0.739±0.034	0.791±0.012	1.830±0.050	1.855±0.535	1.767±0.311
302.8	0.859±0.022	0.860±0.038	2.099±0.164	2.088±0.067	2.168±0.201
356	0.924±0.037	0.929±0.008	3.499±0.572	2.491±0.104	2.442±0.166
383.8	0.957±0.062	1.002±0.004	5.442±3.994	2.900±0.439	2.981±0.252
	Tenth value layer (TVL)				
Energy (keV)	HSS	HSS + 20min	Glass	Glass + 20 min	Glass + 30 min
80.8	0.501±0.004	0.499±0.0002	4.600±0.610	4.851±0.136	4.991±0.181
276.4	2.455±0.112	2.627±0.038	6.083±0.167	6.165±1.777	5.872±1.034
302.8	2.856±0.074	2.859±0.125	6.975±0.545	6.938±0.221	7.206±0.668
356	3.072±0.122	3.088±0.028	11.629±1.902	8.280±0.346	8.117±0.552
383.8	3.181±0.206	3.330±0.012	18.085±13.274	9.637±1.460	9.907±0.838

Table 4. MFPs of the materials and some concretes at 356 keV.

Materials	MFP (cm)
HSS	1.2962
HSS + 20min	1.3325
Glass	5.6336
Glass + 20 min	3.7014
Glass + 30 min	3.3550
Ordinary*	4.3048
Hematite–serpentine*	3.9216
Ilmenite-limonite*	3.4483
Basalt-magnetite*	3.2467
Ilmenite*	2.8604
*[33]	

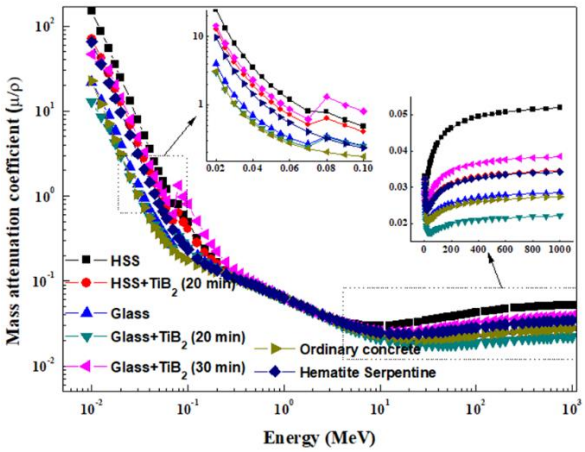

Figure 5. The mass attenuation coefficients (μ/ρ) of investigated materials and some standard shielding concretes.

Exposure buildup factors (EBF) and energy absorption buildup factors (EABF) of the present materials were computed in the 0.05-0.5 MeV photon energy region (at same mfps of 1, 10, 40) as displayed in Figs. 6 and 7. Fig. 6 shows the changes of buildup factors with incident energy at 1, 15, and 40 penetration depths. And it can be said that maximum values (210 and 500 for EBF and EABF) of buildup factors were observed at the largest penetration depth, 40 mfp while minimum values of buildup factors were observed at the lowest penetration depth (1 mfp). EABF and EBF increases as the energy increases on account of the increase in Compton scattering probability of photons at the intermediate energy zone (Figs. 6 and 7).

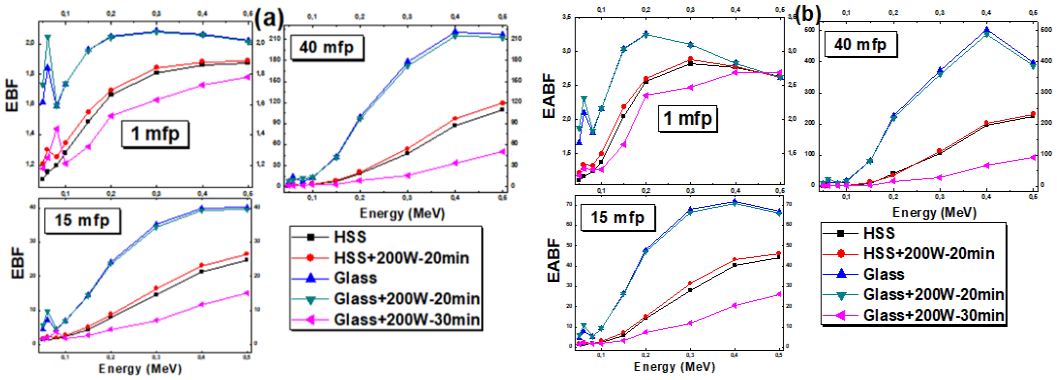

Figure 6. The variation EBF and EABF with incident photon energy (0.05 – 0.5 MeV) at 1, 15, and 40 mfp.

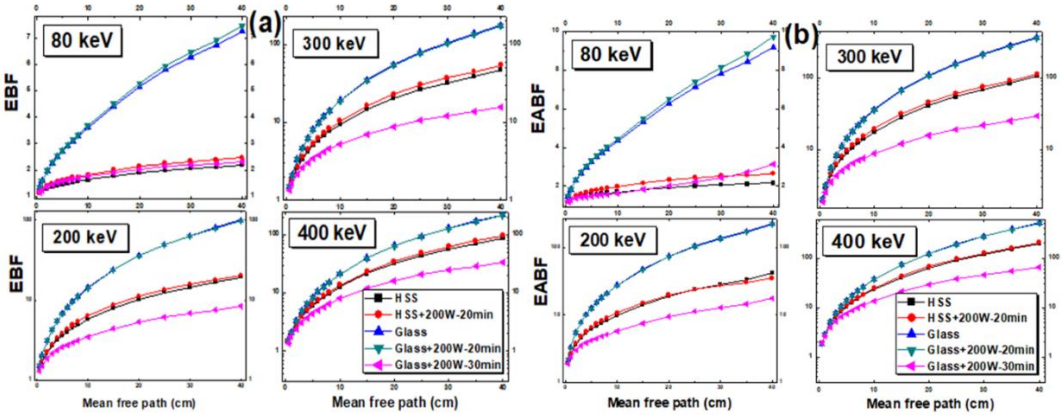

Figure 7. The variation EBF and EABF with penetration depth (up to around 40 mfp) at 80, 200, 300, and 400 keV incident photon energies.

Table 5. Equivalent atomic numbers of the materials at 50-500 keV photon energies.

Energy (keV)	Zeq				
	HSS	HSS+20 Min	Glass	Glass+20 Min	Glass+30 Min
50	25.77	20.75	14.19	13.24	22.20
60	25.82	20.95	14.35	13.46	22.53
80	29.24	26.59	19.70	19.59	35.33
100	29.61	27.25	20.33	20.29	36.34
150	30.22	28.30	21.34	21.41	37.71
200	30.62	28.97	22.00	22.12	38.50
300	31.16	29.80	22.82	23.01	39.58
400	31.49	30.31	23.33	23.55	40.35
500	31.73	30.65	23.67	23.92	40.89

Fig. 7 shows the variation of EBFs and EABFs with the MFPs of the materials at the incident photon energies 80, 200, 300, and 400 keV. It can be shown from the figure that with increasing penetration depths, the EABF and EBF values of the materials increase for given photon energies because of an increase in the number of scattered photons in the materials. Variations of buildup factors with equivalent atomic number (Z_{eq}) were also studied in this work (Table 5). The difference in Z_{eq} values between 60 and 80 keV is due to high Z content i.e. Pt of materials. The K-absorption edge of Pt is around 80 keV which leads to a jump in Z_{eq} values. From Figure 7 and Table 5, it can be clearly seen that buildup factors have lower values for Glass+30 Min, which has a maximum equivalent atomic number, $Z_{eq,}$ while the samples with minimum Z_{eq} (Glass and Glass+20 Min) have higher values of buildup factors. This is because of the fact that the chemical composition of the materials affects attenuation parameters at the investigated photon energies.

4. Conclusion

In the present study, TiB_2 thin films were successfully deposited on HSS and glass substrates. Microstructural investigations revealed that TiB_2 thin films were homogenous and well-adherent with thicknesses between 80 nm and 185 nm. These materials were then investigated in terms of linear attenuation coefficient (μ), half-value layer (HVL), tenth-value layer (TVL), mean free path (MFP), effective atomic number (Z_{eff}) and buildup factors (EBF and EABF) at photon energies 80.8, 276.4, 302.8, 356 and 383.8 keV. Studied materials were also compared with shielding concretes for evaluations. The results showed that TiB_2 coated glass and HSS were better radiation shielding materials than the standard shielding concretes concluding that these materials can be further developed for radiation shielding applications.

References

[1] Munro, R. G. (2000). Material Properties of Titanium Diboride, J. Res. Natl. Inst. Stand. Technol.105:709-720.

[2] Han, Y., Dai, Y., Shu, D., Wang, J., Sun, B. (2007). Electronic and bonding properties of TiB_2. J. Alloys Compd., 438:327-331.

[3] Will, G. (2004). Electron deformation density in titanium diboride chemical bonding in TiB_2.J. Solid. State Chem., 177:628-631.

[4] Telle, R., Sigl, L.S., Takagi, K. (2000). Chapter 7 in Handbook of Ceramic Hard Materials edited by R. Riedel, Wiley-VCH. Weinheim, 879.

[5] Pierson, H.O. (1996). Handbook of Refractory Carbides and Nitrides, Noyes Publications. Westwood, New Jersey, 65.

[6] Huang, F., Barnard, J.A., Weaver, M.L. (2001). Ultrathin TiB_2 protective films. J. Mater. Res.,16(4):945-954.Z., S. Wu, J. Wang, A. Yu and G. Wei, (2019). Carbon nanofiber-based functional nanomaterials for sensor applications. Nanomaterials, 9(7): 1045

[7] Mishra, S. K., Rupa, P.K.P., Pathak, L.C. (2007). Surface and nanoindentation studies on nanocrystalline titanium diboride thin film deposited by magnetron sputtering. Thin Solid Films, 515:6884-6889.

[8] Sanchez, C.M.T., Rebollo Plata, B., Maia da Costa, M.E.H., Freire Jr. F.L. (2011). Titanium diboride thin films produced by dc-magnetron sputtering: Structural and mechanical properties.Surface & Coatings Technology, 205:3698-3702.

[9] Xia, M-j., Ding, H-y., Zhou, G-h., Zhang, Y. (2013). Improvement of adhesion properties of TiB_2 films on 316L stainless steel by Ti interlayer films. Trans. Nonferrous. Met. Soc. China, 23:2957−2961.

[10] Zhang, T.F., Gan, B., Park, S-m., Wang, Q.M., Kim, K.H. (2014). Influence of negative bias voltage and deposition temperature on microstructure and properties of superhard TiB_2 coatings deposited by high power impulse magnetron sputtering. Surface & Coatings Technology, 253:115–122.

[11] Ünsal, Zorla, E., Ipbüker, C., Biland, A., Kiisk, M., Kovaljov, S., Tkaczyk, A.H., Gulik, V. (2017). Radiation shielding properties of high performance concrete reinforced with basalt fibers infused with natural and enriched boron. Nucl. Eng. Des.,313:306-318.

[12] Sharma, A., Reddy, G.R., Varshney, L., Bharathkumar, H., Vaze, K.K., Ghosh, A.K., Kushwaha, H.S., Krishnamoorthy, T.S. (2009). Experimental investigations on mechanical and radiation shielding properties of hybrid lead–steel fiber reinforced concrete. Nucl. Eng.Des., 239:1180-1185.

[13] Tekin, H.O., Singh, V.P., Manici, T. (2017). Effects of micro-sized and nano-sized WO_3 on mass attenauation coefficients of concrete by using MCNPX code. Appl. Radiat. Isot.,121:122-125.

[14] Mostafa, A.M.A., Issa, S.A., Sayyed, M.I. (2017). Gamma ray shielding properties of $PbO-B_2O_3-P_2O_5$ doped with WO_3. J. Alloys Compd., 708:294-300.

[15] Tas, Ersundu, A.E., Büyükyıldız, M., Çelikbilek Ersundu, M., Şakar, E., Kurudirek, M. (2018). The heavy metal oxide glasses within the WO_3 -MoO_3 -TeO_2 system to investigate the shielding properties of radiation applications. Prog. Nucl. Energy, 104:280–287.

[16] Sayyed, M.A., Shams, A.M., Büyükyıldız, M., Dong, M. (2018). Determination of nuclear radiation shielding properties of some tellurite glasses using. Radiat. Phys. Chem., 150:1-8.

[17] Çelikbilek Ersundu, M., Ersundu, A.E., Gedikoğlu, N., Şakar, E, Büyükyıldız, M., Kurudirek, M. (2019). Physical, mechanical and gamma-ray shielding properties of highly transparent $ZnO-MoO_3-TeO_2$. Glasses. J.Non-Crystal Solids, 524:119648.

[18] Akkurt, I., Calik, A., Akyıldırım, H. (2011). The boronizing effect on the radiation shielding and magnetization properties of AISI 316L austenitic stainless steel. Nucl. Eng. Des., 241:55-58.

[19] Büyükyıldız, M., Kurudirek, M., Ekici, M., İçelli, O., Karabul, Y. (2017). Determination of radiation shielding parameters of 304L stainless steel specimens from welding area for photons of various gamma ray sources. Prog. Nucl. Energ., 100:245-254.

[20] Medhat, M.E., Wang, Y. (2015). Investigation on radiation shielding parameters of oxide dispersion strengthened steels used in high temperature nuclear reactor applications. Ann. Nucl. Energy, 80:365-370.

[21] Singh, V.P., Badiger, N.M. (2013). Study of mass attenuation coefficients, effective atomic numbers and electron densities of carbon steel and stainless steels. Radioprotection, 48(3):431-443.

[22] Büyükyıldız, M. (2018). Effect of current intensity on radiological properties of joined 304L stainless steels for photon interaction. Nucl. Sci. Tech. 29: 1-8.

[23] Ipbüker, C. Nulk, H., Gulik, V., Biland, A., Tkaczyk, A.H. (2015). Radiation shielding properties of a novel cement–basalt mixture for nuclear energy applications. Nucl. Eng. Des., 284:27-37.

[24] Karabul, Y., Susam, L.A., İçelli, O., Eyecioğlu, Ö. (2015). Computation of EABF and EBF for basalt rock samples. Nucl. Instrum. Meth. A, 797:29-36.

[25] Jackson, D.F., Hawkes, D.J. (1981). X-ray attenuation coefficients of elements and mixtures,Physics Report. 70:169–233.

[26] Kurudirek, M., Topcuoglu, S. (2011). Investigation of human teeth with respect to the photon interaction, energy absorption and buildup factor. Nucl. Instrum. Meth. B, 269:1071–1081.

[27] İçelli, O., Mann, K.S., Yalçın, Z., Orak, S., Karakaya, V. (2013). Investigation of shielding properties of some boron compounds, Ann. Nucl. Energy, 55:341–350.

[28] Singh, V.P., Badiger, N.M. (2014). The gamma-ray and neutron shielding factors of fly-ash brick materials. J. Radiol. Prot., 34:89–101.

[29] Gerward, L., Guilbert, N., Jensen, K.B., Levring, H. (2004). WinXCom - A program for calculating X-ray attenuation coefficients. Radiat. Phys. Chem., 71:653-654.

[30] Harima, Y. (1993). An historical review and current status of buildup factor calculations and applications. Radiat. Phys. Chem., 41:631-672.

[31] Donnet, C., Fontaine, J., Le Mogne, T., Belin, M., Héau, C., Terrat, J.P., Vaux, F., Pont,G. (1999). Diamond-like carbon-based functionally gradient coatings for space tribology. Surf. Coat. Technol., 120-121:548-554.

[32] Turan, A., Sahin, F.C., Goller, G., Yucel, O. (2014). Spark plasma sintering of monolithic TiB_2 Ceramics. J. Ceram. Process. Res., 15(6):464–468.

[33] *Bashter, I.I. (1997). Calculation of radiation attenuation coefficients for shielding concretes, Ann. Nucl. Energy, 24:11389-1401.